

Three-Dimensional Delayed-Detonation Model of Type Ia Supernova

Vadim N. Gamezo¹, Alexei M. Khokhlov², and Elaine S. Oran¹

ABSTRACT

We study a Type Ia supernova explosion using large-scale three-dimensional numerical simulations based on reactive fluid dynamics with a simplified mechanism for nuclear reactions and energy release. The initial deflagration stage of the explosion involves a subsonic turbulent thermonuclear flame propagating in the gravitational field of an expanding white dwarf. The deflagration produces an inhomogeneous mixture of unburned carbon and oxygen with intermediate-mass and iron-group elements in central parts of the star. During the subsequent detonation stage, a supersonic detonation wave propagates through the material unburned by the deflagration. The total energy released in this delayed-detonation process, $(1.3-1.6) \times 10^{51}$ ergs, is consistent with a typical range of kinetic energies obtained from observations. In contrast to the deflagration model that releases only about 0.6×10^{51} ergs, the delayed-detonation model does *not* leave carbon, oxygen, and intermediate-mass elements in central parts of a white dwarf. This removes the key disagreement between three-dimensional simulations and observations, and makes a delayed detonation the mostly likely mechanism for Type Ia supernova explosions.

Subject headings: supernovae: general — hydrodynamics — nuclear reactions, nucleosynthesis, abundances

¹Laboratory for Computational Physics and Fluid Dynamics, Naval Research Laboratory, Washington, D.C. 20375, gamezo @lcp.nrl.navy.mil, oran @lcp.nrl.navy.mil

²Department of Astronomy and Astrophysics, University of Chicago, Chicago, IL 60637, ajk @oddjob.uchicago.edu

1. Introduction

One-dimensional (1D) numerical models of Type Ia supernovae (SN Ia) have been extensively used to test general ideas about possible explosion mechanisms (Arnett 1969; Hansen & Wheeler 1969; Nomoto et al. 1976; Nomoto et al. 1984; Woosley & Weaver 1986; Wheeler et al. 1995). In particular, 1D models have ruled out the possibility of a thermonuclear detonation, a supersonic shock-induced combustion mode, as a sole mechanism for SN Ia explosions. A detonation propagating through a high-density carbon-oxygen white dwarf (WD) produces mostly Ni and almost none of the intermediate-mass elements, such as Ne, Mg, Si, S, and Ca, that are observed in SN Ia spectra. One-dimensional models have also shown that a detonation can produce intermediate-mass elements if it propagates through a low-density WD preexpanded during the initial deflagration stage of the explosion. These delayed-detonation models (Khokhlov 1991; Yamaoka et al. 1992; Khokhlov et al. 1993; Höflich 1995; Höflich et al. 1995; Höflich & Khokhlov 1996; Niemeyer & Woosley 1998) which have a deflagration-to-detonation transition (DDT) at some stage of the thermonuclear explosion, are the most successful in reproducing observed characteristics of SNe Ia. Many crucial physical details, however, including the mechanism of DDT and the turbulent flame structure, are missing by definition from 1D models because SN Ia explosions are intrinsically three-dimensional (3D) phenomena.

Recent 3D numerical simulations of thermonuclear deflagrations in a WD (Khokhlov 2000; Reinecke et al. 2002a; Reinecke et al. 2002b; Gamezo et al. 2003) demonstrated the importance of 3D effects. In particular, they have shown that the development of a turbulent thermonuclear flame in the gravitational field of a WD allows funnels of unburned and partially burned material to remain in the vicinity of the WD center until the end of the explosion. This would produce distinct signatures of low-velocity carbon, oxygen, and intermediate-mass elements in SN Ia spectra. As the observed spectra do not show these signatures, the predictions of the pure deflagration model are inconsistent with observations. This inconsistency can be resolved if the turbulent flame triggers a detonation that can burn the remaining material near the WD center (Khokhlov 2000; Gamezo et al. 2003; Gamezo et al. 2004). Here, we report results numerical simulations of SN Ia explosions based on a 3D delayed-detonation model. This work extends and clarifies the brief letter (Gamezo et al. 2004) by providing a detailed description of the model and the results, including numerical convergence studies and extended data analysis.

2. Input Physics and Numerical Implementation

The numerical model (Khokhlov 2000; Gamezo et al. 2003) is based on reactive Euler equations that include gravity terms and are coupled with an equation of state for a degenerate matter and a simplified kinetics of energy release. The equations are integrated on a Cartesian adaptive mesh using an explicit, second-order, Godunov-type numerical scheme. The model describes compressible fluid dynamics on large scales in an exploding WD including the expansion of a star, Rayleigh-Taylor (RT) and Kelvin-Helmholtz (KH) instabilities, turbulence, pressure waves, shocks, and detonations. The nuclear kinetics is approximated by a four-equation mechanism (Khokhlov 1991; Khokhlov 2000) that describes the energy release, consumption of carbon, NSE and NSQE relaxations, and neutronization. Appendix A describes details of the nuclear kinetics approximation and explains how it can be used to estimate cumulative mass fractions of major groups of elements.

The model is able to reproduce the two different regimes of the thermonuclear burning in a WD, a subsonic deflagration and a supersonic detonation. These regimes differ by the mechanism of propagation of the reaction wave: a deflagration involves heat conduction or turbulent mixing, and a detonation involves shock compression. For both regimes, the energy is released by the same network of thermonuclear reactions, and the physical thickness of the reaction front strongly depends on density. It can be up to 12 orders of magnitude less than the WD radius R_{WD} for deflagrations (Timmes & Woosley 1992; Khokhlov et al. 1997) and up to 10 orders of magnitude less than R_{WD} for detonations (Khokhlov 1989; Gamezo et al. 1999). Since the large-scale simulations described here do not resolve lengthscales smaller than $10^{-3}R_{WD}$, the reaction fronts at high densities are still unresolved. We explicitly resolve only parts of the reaction zone associated with NSE relaxation that become very large at low densities and cause an incomplete burning that produces Si and other intermediate-mass elements.

Unresolved reaction fronts are treated differently for deflagrations and detonations. For deflagrations, the flame is advanced using a flame-capturing algorithm described in Appendix B that ensures the flame propagation with a prescribed speed. The flame speed is provided by an additional subgrid model (Khokhlov 2000; Gamezo et al. 2003) that takes into account physical processes at scales smaller than the computational cell size. In particular, it assumes that turbulent burning on small unresolved scales is driven by the gravity-induced RT instability. This approach works only if we explicitly resolve enough scales to ensure that the resolved turbulent flame structure corresponds to the flame properties build into the subgrid model. Extensive numerical resolution tests have shown that the minimum computational cell size $\Delta x_{min} = 2.6 \times 10^5$ cm used here for the deflagration stage is adequate for this type of simulation (Gamezo et al. 2003).

For detonations, a front-capturing algorithm and a subgrid model are not needed because the quasi-steady-state velocity of a detonation wave and the equilibrium composition of detonation products do not depend on the kinetics of energy release. We thus can artificially limit the maximum reaction rate in order to increase the reaction-zone thickness to several computational cells and ensure the numerical stability. We implement this by requiring that the mass fraction of carbon should not change by more than 0.1 per timestep. The resulting artificially thick detonation wave described only by reactive Euler equations maintains the correct velocity and burns the material to the equilibrium products regardless of the computational cell size. Resolution tests performed for the detonation stage for $\Delta x_{min} = 10.4 \times 10^5$ cm and 5.2×10^5 cm show no substantial differences in results (see also Fig. 5 and related discussion below). Transient detonation phenomena, such as detonation initiation and extinction, cannot be correctly reproduced without resolving the structure of the detonation wave, and are not included in the simulations.

3. Deflagration Stage

The initial conditions for the deflagration stage model a $1.4M_{\odot}$ WD in hydrostatic equilibrium with initial radius $R_{WD} = 2 \times 10^8$ cm, initial central density $\rho_c = 2 \times 10^9$ g/cm³, spatially uniform initial temperature $T = 10^5$ K, and uniform initial composition with equal mass fractions of ¹²C and ¹⁶O nuclei. The burning was initiated at the center of WD by filling a small spherical region at $r < 0.015R_{WD}$ with hot reaction products without disturbing the hydrostatic equilibrium. We model one octant of the WD assuming mirror symmetry along the $x = 0$, $y = 0$ and $z = 0$ planes. The computational domain is a cube with a side of $x_{max} = 5.35 \times 10^8$ cm.

The development of the thermonuclear flame was described in detail earlier (Gamezo et al. 2003) and is shown in Fig. 1. The initially spherical flame propagates outwards with a laminar velocity ~ 100 km/s, becomes distorted due to the RT instability, and forms multiple plumes at different scales. The flame distortions at small unresolved scales are taken into account by the turbulent subgrid model that controls the normal flame speed. As the flame grows and the star expands, the normal flame speed remains close to ~ 100 km/s, which is small compared to the sound speed 4,000 – 10,000 km/s ahead of the flame. On resolved scales, the flame forms a dynamic convoluted surface penetrated in all directions by very irregular funnels of unburned material. Buoyancy causes the hot, burned, low-density material inside the flame plumes to rise towards the WD surface. The same gravitational forces also pull the cold, unburned, high-density material between the plumes down towards the center. This material continues to burn, but it will not burn out completely as long as convective flows

supply fresh unburned material from outer layers.

At high densities, carbon and oxygen burning produces mostly Ni and other iron-group elements. The energy released increases the temperature of burned material to $\sim 10^{10}$ K and causes the WD to expand. When the density of unburned material becomes lower than $(1 - 5) \times 10^7$ g/cm³, the deflagration begins to produce Si and other intermediate-mass elements. These elements form everywhere along the flame surface, starting from the outer layers reached by the large plumes, and continuing around unburned funnels in the inner parts of the WD. The 3D distribution of elements predicted at 1.94 s after ignition is shown in Fig 2d.

The expansion eventually quenches the burning when the density of unburned material drops below $\simeq 10^6$ g/cm³. The unburned carbon and oxygen remaining between the flame plumes and intermediate-mass elements that form at low densities at different radii are likely to survive the explosion. As we have shown (Khokhlov 2000; Gamezo et al. 2003), this makes predictions of the 3D deflagration model inconsistent with observed spectra of SN Ia.

4. Detonation Stage

The disagreement between predictions from the pure deflagration simulation and observations strongly suggests that the turbulent flame in SN Ia triggers a detonation. The process of DDT involves events occurring at small scales that are comparable to the detonation wave thickness, and, thus, cannot be directly modeled in large-scale simulations. To study the effects of a detonation, we therefore assume a time and a location for DDT. (A similar approach has been used previously in 1D (Khokhlov 1991; Yamaoka et al. 1992; Khokhlov et al. 1993; Höflich 1995; Höflich et al. 1995; Höflich & Khokhlov 1996) and 2D (Arnett & Livne 1994a; Arnett & Livne 1994b; Livne 1999) delayed-detonation models.) We use the deflagration results as initial conditions, and impose a hot spot to ignite the detonation. The time and location for the detonation initiation are parameters that can be varied and optimized. Here, we explore the three cases defined in Table 1.

The frames in the left column of Fig. 1 show the detonation propagation for case (a), which corresponds to central detonation initiation at 1.62 s after the beginning of the deflagration. By that time, the density of unburnt material near the center has dropped to 2.5×10^8 g/cm³. A detonation at this density produces mostly Ni and propagates outwards at $\sim 12,000$ km/s, which is comparable to the expansion velocities induced by subsonic burning. When the detonation reaches unburned material with density below $(1 - 5) \times 10^7$ g/cm³, it

Table 1: Parameters of a WD at the time detonation initiation (t^{di}) for delayed-detonation cases computed: burned mass fraction (f_b^{di}), density of unburned material near the WD center (ρ^{di}), WD radius (R_{WD}^{di}), maximum distance from the flame surface to the WD center (R_f^{di}), distance from the initiation point to the WD center (R^{di}). Symmetry boundary conditions imply that the off-center initiation in case (b) occurs at two points.

Case	t^{di}	f_b^{di}	ρ^{di}	R_{WD}^{di}	R_f^{di}	R^{di}
			10^8	10^8	10^8	10^8
	s		g/cm^3	cm	cm	cm
a	1.62	0.33	2.5	3.1	2.3	0
b	1.62	0.33	2.5	3.1	2.3	1
c	1.51	0.25	4.4	2.6	1.7	0

begins to produce intermediate-mass elements. Different parts of the detonation front that exit different funnels collide with each other, coalesce, and eventually reach the surface of the star.

The detonation transforms all carbon and oxygen in central parts the WD into iron-group elements, and produces intermediate-mass elements in outer layers. This drastically changes the distribution of nuclei compared to that produced by the pure deflagration. Figure 2a shows that funnels of unburned carbon and oxygen disappear from central parts of the WD. Iron-group elements form a distinct core surrounded by a layer of intermediate-mass nuclei. Angle-averaged mass fractions of the main elements calculated for the deflagration and the delayed-detonation models as functions of distance from the WD center are compared in Fig. 3.

Similar results were obtained for the delayed-detonation case (c) with earlier central initiation at 1.51 s. The detonation starts in the material with density $4.4 \times 10^8 \text{ g/cm}^3$ propagates outwards, and almost completely covers the flame plumes by 1.82 s, as shown in the right column of Fig. 1. By that time, that corresponds to Figs. 2c, 3c, and 4c, the shock already reached the WD surface, burned almost all of the carbon, and left unburned oxygen in low-density outer layers. The integral mass distribution of the main elements in Fig. 4 shows that case (c) produced more iron-group elements than case (a) because the detonation propagated through higher-density material. Figure 2c shows that iron-group elements form a more compact core because the flame plumes had less time to develop. Intermediate-mass elements also form a more distinct shell with a higher Si peak in Fig. 3c. Thus, the earlier detonation initiation results in more symmetrical, shell-like distribution of elements.

Cases (a) and (c) were computed with two different numerical resolutions with $\Delta x_{min} =$

10.4×10^5 cm and 5.2×10^5 cm. Total energies for these cases are shown in Fig. 5 as functions of time. Dotted lines correspond to the lower resolution and show a slightly lower energy release compared to high-resolution results. The difference (6% for the case (a) and 3% for the case (c)) is insignificant and related to small pockets of unburned material that remain behind the shock propagating through the turbulent flame in low-resolution simulations.

The delayed-detonation case (b) was computed only with the low resolution ($\Delta x_{min} = 10.4 \times 10^5$ cm). This case is interesting because it shows asymmetrical effects created by an off-center detonation initiation. The simulation results for this case show a moderate asymmetry in final composition. The asymmetry is limited because we calculate only one octant of a WD and impose mirror boundary conditions. The degree of asymmetry would increase if the simulations were performed for a full star. Then the second mirror-reflected spot for detonation initiation would be eliminated. The simulation results indicate that, during the period of detonation propagation, the density of the expanding unreacted material ahead of the shock can decrease by an order of magnitude compared to its value at the end of the deflagration stage. Because the detonation burns material to different products at different densities, it can create a large-scale asymmetry in composition if it starts far from the WD center. A similar conclusion based on 2D simulations was made by (Livne 1999). Three-dimensional simulations of the deflagration stage (Khokhlov 2000; Calder et al. 2003) also show that a developing flame, unrestricted by mirror boundaries, can move away from the WD center, thus creating a large-scale asymmetry at very early stages of the explosion.

5. Discussion and Conclusions

The first result that can be compared to observations is the energy released by the explosion. Total energies for all three delayed-detonation cases and the deflagration model are compared in Fig. 5. The total energy E_{tot} here is the difference between the energy released by thermonuclear reactions and the binding energy of the star. Eventually E_{tot} will be transformed into kinetic energy of expanding material that can be measured in observations of SN Ia. Figure 5 shows that the total energy predicted by delayed-detonation models, $(1.3 - 1.6) \times 10^{51}$ ergs, is much higher than the total energy predicted by the deflagration model $\sim 0.6 \times 10^{51}$ ergs. The reason for this is that the deflagration is able to burn only about a half of the WD mass. The rest of the material expands to the densities below $\simeq 10^6$ g/cm³ that do not support the thermonuclear burning. A detonation propagates faster and burns almost all of the WD mass before the material expands to low densities. A small difference in energy curves plotted in Fig. 5 for the delayed-detonation cases (a) and (b) indicates that the off-center detonation initiation in this model has only a minor effect on

the energy release. Case (c), with earlier detonation initiation, resulted in a faster explosion that released 15% more energy. The total energy released by the delayed-detonation models is in agreement with a typical range $(1 - 1.5) \times 10^{51}$ ergs obtained from SN Ia observations (Wheeler et al. 1995).

Another result that can be compared to observations is the total mass of radioactive ^{56}Ni that provides the energy source for the observed luminosity of SN Ia. The simplified kinetic model we use in these simulations does not provide the exact concentration of ^{56}Ni , but it gives a cumulative concentration of iron-group elements, most of which is ^{56}Ni . By the end of each simulation described here, all iron-group elements that could form during the explosion have already formed. Even though some material is still burning and releasing energy for cases (a), (b), and (d) (see Fig. 5), the burning occurs at low densities and produces mostly intermediate-mass elements. The total mass of iron-group elements created by the explosion (see Fig. 4) is 0.78, 0.73, and 0.98 solar masses (M_{\odot}) for delayed-detonation cases (a), (b), and (c), respectively. The mass of ^{56}Ni estimated from observational data is about $0.6M_{\odot}$ for a typical SN Ia (Branch & Khokhlov 1995), and is in agreement with the total mass of iron-group elements produced by delayed-detonation models. For the deflagration model, the total mass of iron-group elements is only $0.47 M_{\odot}$, which is insufficient to account for the luminosity of a typical SN Ia.

Distributions of carbon, oxygen, and intermediate-mass elements predicted by the models also can be checked against observations. In the simulations, detonations burn all carbon and oxygen in inner parts of WD. Oxygen remains unburned in outer layers, which expand to densities below $\simeq 10^6$ g/cm³ before the detonation reaches them. Carbon is likely to remain unburned for densities below $(1 - 3) \times 10^5$ g/cm³. These unburned carbon and oxygen in outer layers would produce spectral signatures only in the high-velocity range.

There are ways in which a delayed detonation can leave small amounts of carbon and oxygen in inner parts of WD. For example, a detonation propagating through a thin, sinuous funnel of unburned material can fail if the funnel makes a sharp turn. This detonation failure occurs as a result of detonation diffraction process that is well-known for terrestrial systems. A developing turbulent flame can also disconnect some funnels from the rest of the unburned material, thus creating unburned pockets that cannot be directly reached by a detonation wave. Some of these pockets may not ignite when strong shocks generated by detonations reach them. The cellular structure of thermonuclear detonations in carbon-oxygen matter (Gamezo et al. 1999), and the ability of cellular detonations to form pockets of unburned material that extend far behind the 1D reaction zone, can also contribute into incomplete burning. All these phenomena occur at lengthscales comparable to the reaction zone thickness that are not resolved in large-scale simulations reported here, and thus require

additional studies.

There have recently been efforts to detect low-velocity carbon in SN Ia spectra that could result from the funnels of unburned material near the WD center (Branch et al. 2003). The results (Branch et al. 2003) indicate that carbon can be present at velocities 11,000 km/s. Even though this velocity is much lower than 20,000-30,000 km/s usually attributed to carbon in SN Ia spectra (Kirshner et al. 1993; Fisher et al. 1997; Mazzali 2001), it is still too high for the ejecta formed from central parts of a WD. For carbon and oxygen, spectral signatures are difficult to observe, and estimated velocities of these elements are subject to large uncertainties. Intermediate-mass elements, however, produce distinct spectral lines and their velocities are well defined. The minimum observed velocities for intermediate-mass elements (Branch et al. 2003; Filippenko 1997) are large enough ($\sim 10,000$ km/s for Si) to rule out the presence of these elements near the WD center, as is predicted by the deflagration model. A discussion on this subject can also be found in the recent article by (Branch 2004).

Figures 2-4 show that, in contrast to the 3D deflagration model, the 3D delayed-detonation model of SN Ia explosion does *not* leave carbon, oxygen, and intermediate-mass elements in central parts of a WD. This removes the key disagreement between simulations and observations, and makes the 3D delayed detonation a promising mechanism for SN Ia explosion. Further analysis of 3D delayed detonations on large scale requires 3D radiation transport simulations to produce spectra, and a detailed comparison between the calculated and observed spectra of SN Ia for different initiation times and locations. The uncertainty in detonation initiation can only be eliminated by solving the DDT problem that requires resolving physical processes at small scales.

This work was supported in part by the NASA ATP program (NRA-02-OSS-01-ATP) and by the Naval Research Laboratory (NRL) through the Office of Naval Research. Computing facilities were provided by the DOD HPCMP program. We would like to thank Peter Höflich and J. Craig Wheeler for useful discussions.

A. Nuclear Kinetics

Nuclear reactions involved in the thermonuclear burning of the carbon-oxygen mixture (Fowler et al. 1975; Woosley et al. 1978; Thielemann et al. 1987) can be separated into three consecutive stages responsible for the energy release. First, the $^{12}\text{C} + ^{12}\text{C}$ reaction leads to the consumption of C and formation of mostly Ne, Mg, protons, and α -particles. Then begins the nuclear statistical quasi-equilibrium (NSQE) relaxation, during which O burns

out and Si-group (intermediate mass) elements are formed. Finally, Si-group elements are converted into the Fe-group elements and the nuclear statistical equilibrium (NSE) sets in. The reaction time scales $\tau_C \ll \tau_{nsqe} \ll \tau_{nse}$ associated with these stages strongly depend on temperature and density and may differ from one another by several orders of magnitude (Truran et al. 1966; Bodansky et al. 1968; 1; Khokhlov 1989; Gamezo et al. 1999).

The full nuclear reaction network includes hundreds of species that participate in thousands of reactions. Integration of this full network is too time-consuming to be used in multidimensional numerical models. Therefore, we used a simplified four-equation kinetic scheme (Khokhlov 1991; Khokhlov 2000) that describes the energy release, NSE and NSQE relaxations, and neutronization of NSE matter.

The kinetic equation for the mole fraction of carbon Y_C

$$\frac{dY_C}{dt} = -\rho A(T_9) \exp(-Q/T_{9a}^{1/3}) Y_C^2, \quad (\text{A1})$$

describes carbon consumption through the major reactions $^{12}\text{C} (^{12}\text{C}, p) ^{23}\text{Na} (p, \gamma) ^{24}\text{Mg}$ and $^{12}\text{C} (^{12}\text{C}, ^4\text{He}) ^{20}\text{Ne}$ with the branching ratio $\simeq 1$. Here $Q = 84.165$, $T_{9a} = T_9/(1 + 0.067T_9)$, where $A(T_9)$ is a known function (Fowler et al. 1975).

Most of the nuclear energy is released during the carbon exhaustion stage and the subsequent synthesis of the Si-group nuclei. The energy release or consumption due to the transition from Si-group to Fe-group nuclei (NSE relaxation) is less than 10%. Therefore, the nuclear energy release rate is approximated as

$$\frac{dq_n}{dt} = -Q_C \frac{dY_C}{dt} + \frac{q_{nse} - q_n}{\tau_{nsqe}}, \quad (\text{A2})$$

where $q_n(t)$ is the binding energy of nuclei per unit mass, $Q_C = 4.48 \times 10^{18}$ ergs $\text{g}^{-1} \text{mol}^{-1}$ is the energy release due to carbon burning described by Eq. (A1), and $q_{nse}(\rho, T, Y_e)$ is the binding energy of matter in the state of NSE.

The equation

$$\frac{d\delta_{nse}}{dt} = \frac{1 - \delta_{nse}}{\tau_{nse}}, \quad (\text{A3})$$

traces the onset of NSE, where $\delta_{nse} = 0$ in the unburned matter and $\delta_{nse} = 1$ in the NSE products. Intermediate mass elements are expected where $Y_C(t = \infty) \simeq 0$ and $\delta_{nse}(t = \infty) < 1$. Fe-group elements are expected where $Y_C(t = \infty) \simeq 0$ and $\delta_{nse}(t = \infty) \simeq 1$. The ‘e-folding’ NSQE and NSE timescales

$$\tau_{nsqe} = \exp(149.7/T_9 - 39.15) \text{ s}, \quad \tau_{nse} = \exp(179.7/T_9 - 40.5) \text{ s}, \quad (\text{A4})$$

approximate the results of the detailed calculations of carbon burning.

Neutronization is described by the equation for the electron mole fraction Y_e ,

$$\frac{dY_e}{dt} = -R_w(\rho, T, Y_e) . \quad (\text{A5})$$

The corresponding term describing neutrino energy losses, $-\dot{q}_w(\rho, T, Y_e)$, is added to the nuclear energy release rate used in reactive Euler equations. Values of q_{nse} , \dot{q}_w , and R_w were computed assuming NSE distribution of individual nuclei, as described in (Khokhlov 1991). Recently, there has been an important development in theoretical computations which shows significantly smaller electron capture and β -decay rates in stellar matter ((Langanke & Martinez-Pinedo 1998 and references therein). Following (Martinez-Pinedo et al. 2000), this effect was approximately taken into account by decreasing \dot{q}_w and R_w by a factor of 5. This should be sufficient to account for changes in q_{nse} and in the corresponding nuclear energy release $q_{nse} - q_n(t = 0)$ caused by variations of Y_e .

The original kinetic scheme (Khokhlov 1991) also contained the equation for the mean ion mole fraction Y_i . Here we neglect variations of Y_i due to nuclear reactions since ions make a small contribution to the equation of state. A constant $Y_i = 0.07$ was used instead, which is an average of Y_i in the unburned and typical NSE matter in the SN Ia explosion conditions.

Despite its simplicity, the kinetic scheme adequately describes all major stages of the thermonuclear burning in a carbon-oxygen WD. In particular, it takes into account the important effect of energy release or absorption caused by changes in NSE composition when matter expands or contracts (these changes happen on a quasi-equilibrium rather than on the equilibrium timescale). When the WD expands, this effect adds $\simeq 50\%$ to the energy initially released by burning at high densities. Using even the simplest 13-species α -network to account for this effect would be prohibitively expensive in 3D simulations of SN Ia explosions. The same kinetic scheme was used in (Khokhlov 2000; Gamezo et al. 2003) for the deflagration stage, but the nuclear energy release was overestimated by about 17% due to an incorrect numerical implementation. Here we use a corrected model that produces slightly slower and less energetic deflagrations.

The mass fraction of carbon X_C and the NSE progress variable δ_{nse} provided by the kinetic scheme were used to estimate cumulative mass fractions of iron-group elements X_{Ni} , intermediate-mass elements X_{Si} , elements from Mg to Ne X_{Mg} , and a mass fraction of oxygen X_O , assuming that $X_C + X_O + X_{Mg} + X_{Si} + X_{Ni} = 1$. The estimation scheme summarized in Table 2 is based on the analysis of the reaction zone structure of a 1D detonation wave calculated in (Khokhlov 1989) with a detailed nuclear kinetics. The estimated mass fractions were not involved in fluid dynamics simulations and used only for the analysis of the simulation results.

Table 2: Estimation scheme for mass fractions of main elements.

Mass fraction	$X_C > \delta_s$	$X_C < \delta_s$ $\delta_{nse} < \delta_s$	$X_C < \delta_s$ $\delta_{nse} > \delta_s$
X_O	X_O^0	$X_O^0(1 - \delta_{nse}/\delta_s)$	0
X_{Mg}	$(X_C^0 - X_C)/2$	$(X_C^0 - X_C)(1 - \delta_{nse}/\delta_s)/2$	0
X_{Si}	X_{Mg}	$(X_C^0 - X_C)/2 + (1 - (X_C^0 + X_C)/2)\delta_{nse}/\delta_s$	$1 - \delta_{nse}$
X_{Ni}	0	0	$\delta_{nse} - X_C$

X_C^0 and X_O^0 are initial mass fractions of carbon and oxygen, $\delta_s = 0.001$.

B. Flame propagation

The flame speed S in our simulations is provided by a subgrid model (Khokhlov 2000; Gamezo et al. 2003) that takes into account physical processes at scales smaller than the computational cell size. The flame is advanced using a flame-capturing technique which mimics a flame propagating with a prescribed normal speed (Khokhlov 1995; Khokhlov 2000; Gamezo et al. 2003). A scalar variable f , such that $f = 0$ in the unburned matter and $f = 1$ in the material which has passed through the flame, obeys a reaction-diffusion equation

$$\frac{\partial f}{\partial t} + \mathbf{U} \cdot \nabla f = K \nabla^2 f + R, \quad (\text{B1})$$

with artificial reaction and diffusion coefficients

$$K = \text{const}, \quad R = \begin{cases} C = \text{const.}, & \text{if } f_0 \leq f \leq 1; \\ 0, & \text{otherwise,} \end{cases} \quad (\text{B2})$$

where $f_0 = 0.3$. Equation (B1) has a solution $f(x - St)$ which describes a reaction front that propagates with the speed $S = (KC/f_0)^{1/2}$ and has a thickness $\delta \simeq (K/C)^{1/2}$ (see Appendix of (Khokhlov 1995)). If K and C in Eq. (B2) are set to

$$K = S(\beta \Delta x) \sqrt{f_0}, \quad C = \frac{S}{(\beta \Delta x)} \sqrt{f_0}, \quad (\text{B3})$$

with $\beta = \text{const}$, the front propagates with a prescribed speed S and spreads onto several computational cells of size Δx . The choice of $\beta = 1.5$ spreads the flame on $\simeq 3-4$ cells.

Making the front narrower is not practical, since the fluid dynamics algorithm spreads contact discontinuities on $\simeq 4$ cells.

To couple Eq. (B1) and the nuclear kinetic scheme described in Appendix A, the energy-release rate inside the front is defined as

$$\dot{q} = q_f \frac{df}{dt}, \quad (\text{B4})$$

where the nuclear energy release inside the front q_f is calculated depending on the density as:

$$q_f = \begin{cases} q_{nse} - q_n(0) & \text{if } \rho > 2 \times 10^7 \text{ g/cm}^3 \\ Q_C Y_C(t=0) & \text{if } \rho < 5 \times 10^6 \text{ g/cm}^3 \\ \text{linear interpolation} & \text{if otherwise} \end{cases} \quad (\text{B5})$$

The carbon mole fraction Y_C inside the front is decreased in proportion to the increase of f . Thus, at high densities, both carbon consumption and the NSQE relaxation take place inside the flame front. At low densities where the NSQE stage of burning is slow, NSQE relaxation takes place outside the flame front. This flame-capturing technique advances the reaction front relative to the fuel with the speed practically independent of the orientation of the front on the mesh, fluid motions, and resolution.

REFERENCES

- Arnett, W. D. 1969, *Ap&SS*, 5, 180
- Arnett, D. & Livne, E. 1994, *ApJ*, 427, 315
- Arnett, D. & Livne, E. 1994, *ApJ*, 427, 330
- Bodansky, D., Clayton, D. D., & Fowler, W. A. 1968, *ApJS*, 16, 299
- Branch, D. & Khokhlov, A. M. 1995, *Phys. Rep.* 256, 53
- Branch, D. et al. 2003, *AJ*, 126, 1489
- Branch, D. 2004, in *3-D Signatures in Stellar Explosions*, in press (astro-ph/0310685).
- Calder, A. C. et al. 2003, *BAAS*, 35, #5
- Filippenko, A. V. 1997, *ARA&A*, 35, 309
- Fisher, A., Branch, D., Nugent, P. & Baron, E. 1997, *ApJ*, 481, L89

- Fowler, W. A., Caughlan, G. R. & Zimmerman, B. A. 1975, *ARA&A*, 13, 69
- Gamezo, V. N., Khokhlov, A. M. & Oran, E. S. 2004, *Phys. Rev. Lett.*, 92, 211102
- Gamezo, V. N., Khokhlov, A. M., Oran, E. S., Chtchelkanova, A. Y. & Rosenberg, R. O. 2003, *Science*, 299, 77
- Gamezo, V. N., Wheeler, J. C., Khokhlov, A. M. & Oran, E. S. 1999, *ApJ*, 512, 827
- Hansen, C. J. & Wheeler, J. C. 1969, *Ap&SS*, 3, 464
- Höflich, P. A. 1995, *ApJ*, 443, 89
- Höflich, P. A., Khokhlov, A. M. & Wheeler, J. C. 1995, *ApJ*, 444, 831
- Höflich, P. A. & Khokhlov, A. M. 1996, *ApJ*, 457, 500
- Khokhlov, A. M. 1991, *A&A*, 245, 114
- Khokhlov, A. M., Müller, E. & Höflich, P. A. 1993, *A&A*, 270, 223
- Khokhlov, A. M. 2000, *astro-ph/0008463*
- Khokhlov, A. M., Oran, E. S. & Wheeler, J. C. 1997, *ApJ*, 478, 678
- Khokhlov, A. M. 1989, *MNRAS*, 239, 785
- Khokhlov, A. M. 1995, *ApJ*, 449, 695
- Kirshner, R. P. et al. 1993, *ApJ*, 415, 589
- Langanke, K. & Martinez-Pinedo, G. 1999, *Phys. Lett. B*, 453, 187
- Livne, E. 1999, *ApJ*, 527, L97
- Martinez-Pinedo, G., Langanke, K., & Dean, D. J. 2000, *ApJ*, 126, 493
- Mazzali, P. A. 2001, *MNRAS*, 321, 341
- Niemeyer, J. C. & Woosley, S. E. 1997, 475, 740
- Nomoto, K., Sugimoto, D. & Neo, S. 1976, *Ap&SS*, 39, L37
- Nomoto, K., Thielemann, F.-K. & Yokoi, K. 1984, *ApJ*, 286, 644
- Reinecke, M., Hillebrandt, W. & Niemeyer, J. C. 2002, *A&A*, 386, 936

- Reinecke, M., Hillebrandt, W. & Niemeyer, J. C. 2002, *A&A*, 391, 1167
- Thielemann, F.-K., Arnould, M., & Truran, J. W. 1987, in *Advances in Nuclear Astrophysics*, ed, E. Vangioni-Flam, (Editions frontières, Gif-sur-Yvette), 525
- Timmes, F. X. & Woosley, S. E. 1992, *ApJ*, 396, 649
- Truran, J. W., Cameron, A. G. W., & Gilbert, A. 1966, *Canadian J. of Phys.*, 44, 563
- Wheeler, J. C., Harkness, R. P., Khokhlov, A. M. & Höflich, P. A. 1995, *Phys. Rep.*, 256, 211
- Woosley, S. E., Arnett, W. D., & Clayton, D. D. 1973, *ApJS*, 26, 231
- Woosley, S. E., Fowler, W. A., Holmes, J. A. & Zimmerman, B. A. 1978, *Atomic Data and Nuclear Data Tables*, 22, 371
- Woosley, S. E. & Weaver, T. A. 1986, *ARA&A*, 24, 205
- Yamaoka, H., Nomoto, K., Shigeyama, T. & Thielemann, F.-K. 1992, *ApJ*, 393, L55

Fig. 1.— Development of a turbulent thermonuclear flame (colored surface) and a detonation (gray surface) in a carbon-oxygen WD. Numbers show time in seconds after ignition. Central column shows the deflagration stage. Left and right columns correspond to delayed-detonation cases (a) (detonation starts at 1.62 s) and (c) (detonation starts at 1.51 s), respectively. Flames at 0.30, 0.61, 0.90, and 1.20 s are plotted at the same scale. Further flame growth is shown by the color scale that changes with distance from the flame surface to the WD center. $x_{max} = 5.35 \times 10^8$ cm.

Fig. 2.— Concentration field in the exploding WD computed for deflagration (d) and delayed-detonation (a,c) models defined in Table 1. Times are 1.94, 1.94, and 1.82 s for cases d, a, and c, respectively. The color map shows the average atomic number A of the material for $x = 0.05$, $y = 0.05$, and $z = 0.05$ planes. The coordinate grid is spaced by $0.2x_{max}$. $A = \sum X_i A_i$, where X_i are mass fractions of C, O, Mg, Si, Ni defined in Appendix A.

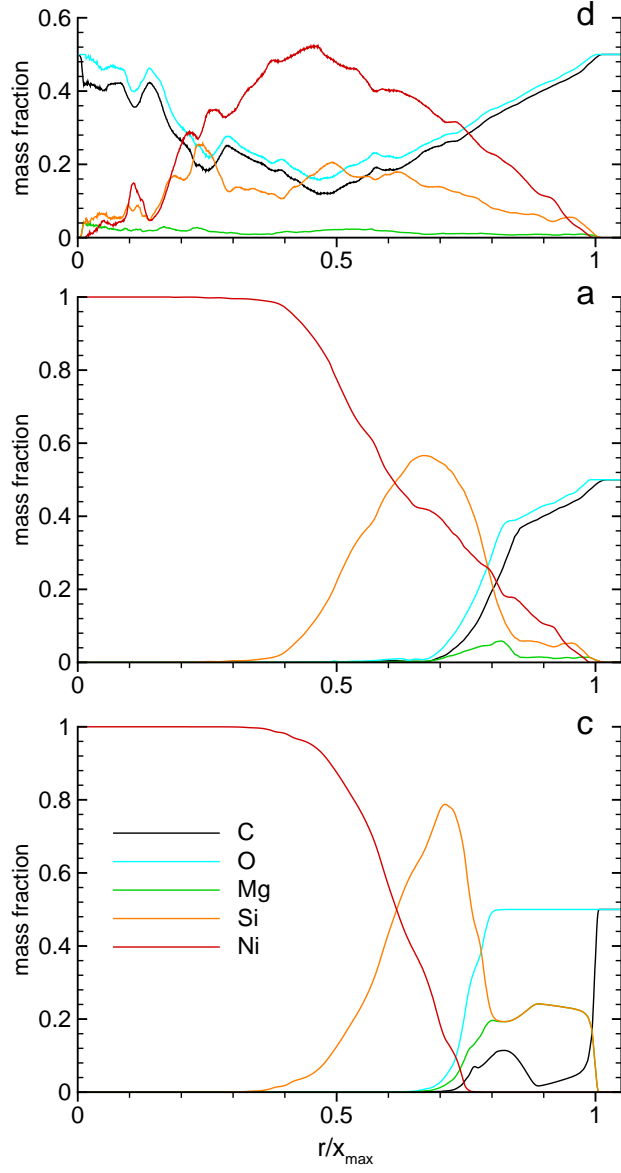


Fig. 3.— Angle-averaged mass fractions of the main elements as functions of scaled distance from the WD center produced by the deflagration (d) and delayed-detonation (a,c) models defined in Table 1. Times are 1.94, 1.94, and 1.82 s after the beginning of the explosion for cases d, a, and c, respectively. $x_{max} = 5.35 \times 10^8$ cm.

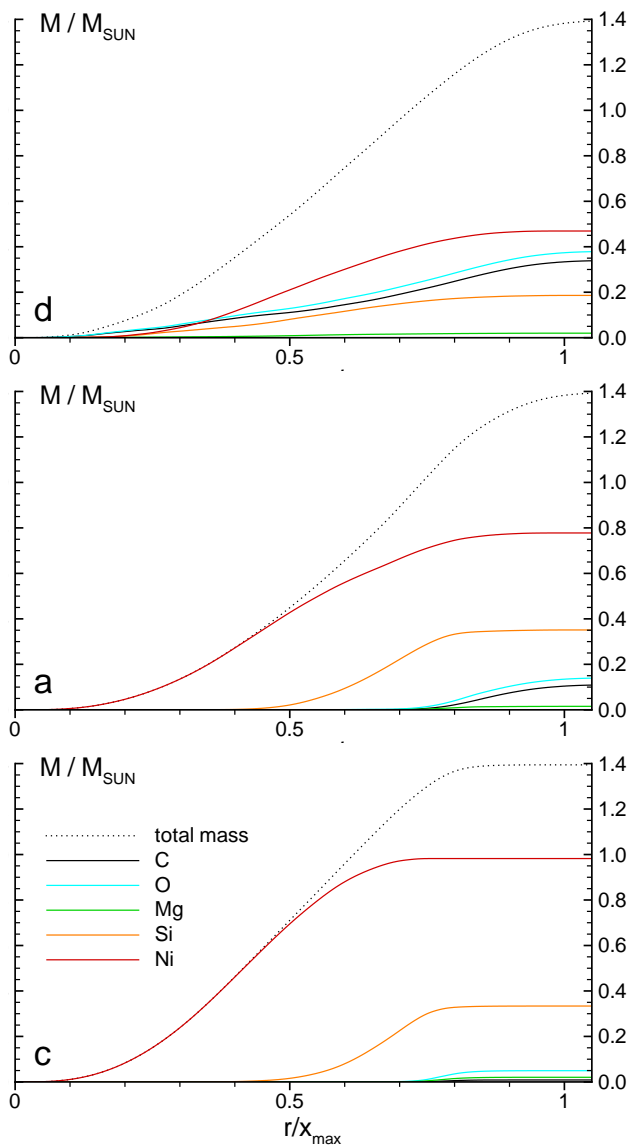


Fig. 4.— Integral mass distribution of the main elements in the exploding WD produced by the deflagration (d) and delayed-detonation (a,c) models defined in Table 1. Times are 1.94, 1.94, and 1.82 s after the beginning of the explosion for cases d, a, and c, respectively. The mass is scaled by the solar mass, the radius is scaled by the computational domain size $x_{\text{max}} = 5.35 \times 10^8$ cm.

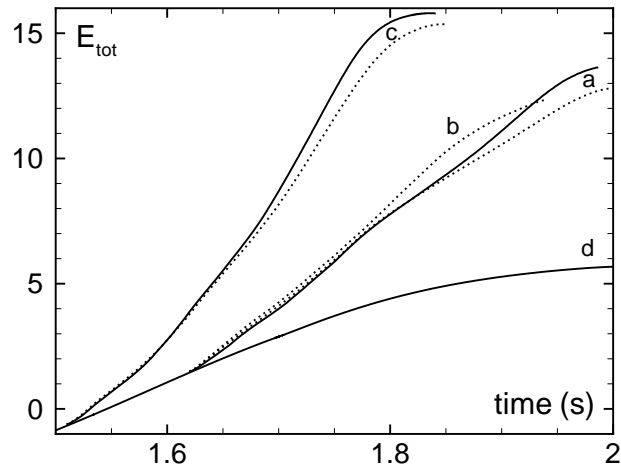


Fig. 5.— Total energy as function of time for deflagration (d) and delayed-detonation cases a, b, c listed in Table 1. Dotted lines correspond to low-resolution simulations. Energy units are 10^{50} ergs.

This figure "fig1.jpg" is available in "jpg" format from:

<http://arxiv.org/ps/astro-ph/0409598v1>

This figure "fig2.jpg" is available in "jpg" format from:

<http://arxiv.org/ps/astro-ph/0409598v1>